Characterization of the Metal Ion-Binding Domains from Rat α- and β-Parvalbumins†

Michael T. Henzl,* Sayeh Agah, and John D. Larson

Department of Biochemistry, University of Missouri−Columbia, Columbia, Missouri 65211

Received October 24, 2002; Revised Manuscript Received January 5, 2003

ABSTRACT: We have examined the metal ion-binding domains from rat α and β parvalbumin. We find that the CD-EF fragments differ markedly in their tendency to self-associate. Whereas Ca^{2+}-free α CD-EF is monomeric, the Ca^{2+}-free β peptide dimerizes weakly ($K_2 = 2400 \pm 200\ M^{-1}$). In buffer containing 1.0 mM Ca^{2+}, the apparent dimerization constant for β CD-EF ($191\,000 \pm 29\,000\ M^{-1}$) is more than 50 times that of α ($3400 \pm 200\ M^{-1}$). α CD-EF binds two Ca^{2+} with positive cooperativity. Titration calorimetry data afford binding constants of $3.7(0.1) \times 10^3\ M^{-1}$ and $8.6(0.2) \times 10^4\ M^{-1}$. β CD-EF also binds two Ca^{2+} cooperatively but with lower affinity. Equilibrium dialysis yields Adair constants of $4.2(0.1) \times 10^3$ and $6.1(0.2) \times 10^3\ M^{-1}$. Significantly, the difference in Ca^{2+} affinity is substantially smaller than that observed for the full-length proteins—suggesting that the AB domain can modulate divalent ion affinity. Analysis of β calorimetry data requires explicit consideration of the self-association behavior. Data collected at low CD-EF concentration are consistent with preferential occupation of the EF site, dimerization of singly bound monomers, and cooperative filling of the CD sites. At higher concentrations, apo-protein dimerization can apparently precede cooperative occupation of the EF sites. In the presence of Ca^{2+}, α CD-EF exhibits higher thermal stability, consistent with its higher Ca^{2+} affinity. However, the β melting temperature shows greater concentration dependence, consistent with its greater tendency to dimerize. Neither fragment exhibits a sigmoidal melting curve in the Ca^{2+}-free state, suggesting that the apo-peptides are disordered.

The critical role of Ca^{2+} in signal transduction is mediated by a host of Ca^{2+}-binding proteins. Many of these contain a characteristic Ca^{2+}-binding motif, the EF-hand, which consists of a central ion-binding loop flanked by short helical elements (*1*, *2*). Within the binding loop, the ligands assume a roughly octahedral arrangement about the bound ion and are indexed by the axes of a Cartesian coordinate system: $+x$, $+y$, $+z$, $-y$, $-x$, and $-z$. The $-y$ ligand is a main-chain carbonyl; $-x$ is frequently water; and $-z$ is glutamate. The remaining ligands are side-chain oxygen atoms—carboxylate, carbonyl, or hydroxyl. Because Ca^{2+} ligation at $-z$ is bidentate, the coordination is actually pentagonal bipyramidal.

Despite the similarity of their metal ion-binding sites, individual EF-hand proteins exhibit large differences in Ca^{2+} affinity (*3*). The structural basis for these variations is of great interest. Our efforts in this structure−affinity arena have focused on the rat α and β parvalbumins.

Parvalbumins are small, vertebrate-specific Ca^{2+}-binding proteins believed to function as Ca^{2+} buffers (*1*, *2*, *4*). The parvalbumin (PV)[1] tertiary structure, first determined by Kretsinger and Nockolds (*5*), includes a 40-residue N-terminal domain (the AB domain) fused to a 70-residue metal ion-binding domain (the CD-EF domain). The latter harbors two EF-hand metal ion-binding motifs (the CD and EF sites). The PV family includes two sublineages, α and β, distinguished by isoelectric point (α ≥ 5), C-terminal helix length (generally one residue longer in α), and several lineage-specific sequence assignments (e.g., cys-18 in β) (*6*, *7*). Mammals express one isoform from each lineage (*8*). The α isoform is expressed in various tissues, notably fast-twitch muscle fibers and GABA-ergic neurons, where it probably serves to modulate the amplitude and duration of Ca^{2+} transients (*9*−*11*). To date, β has been detected in postnatal mammals solely in the outer hair cells (*12*, *13*)—highly specialized cells of the auditory organ that function in the amplification of weak acoustic signals. Its physiological role is presently unknown.

Although rat α and β exhibit 49% sequence identity (*14*, *15*), they display distinct divalent ion-binding properties.

† This work was supported by NSF award MCB-0131166 (to M.T.H.). The Beckman Optima XL-I used for these studies was purchased with funds from NSF award DBI-9604733 and the University of Missouri PRIME fund. Portions of this work were presented at the 57th Calorimetry Conference, August 11−15, 2002 in New Brunswick, NJ and at the 16th Annual Gibbs Conference on Biothermodynamics, September 29 through October 1, 2002 in Carbondale, IL.

* Corresponding author. E-mail: henzlm@missouri.edu.

[1] Abbreviations: CD, circular dichroism; CD site, parvalbumin metal ion-binding site flanked by the C and D helical segments; DEAE, diethylaminoethyl; EDAC, 1-ethyl-3-(3-dimethylaminopropyl)carbodiimide; EDTA, ethylenediaminetetraacetic acid; EF site, parvalbumin metal ion-binding site flanked by the E and F helical segments; EGTA, ethylene glycol-bis(β-aminoethyl ether)-*N*,*N*,*N*′,*N*′-tetraacetic acid; GABA, γ-aminobutyric acid; Hepes, 4-(2-hydroxyethyl)-1-piperazineethanesulfonic acid; IPTG, isopropyl β-D-thiogalactoside; ITC, isothermal titration calorimetry; LB, Luria−Bertani; NLLS, nonlinear least squares; NMR, nuclear magnetic resonance; NTA, nitrilotriacetic acid; PAGE, polyacrylamide gel electrophoresis; PCR, polymerase chain reaction; PV, parvalbumin; TnC, troponin C.

10.1021/bi027060x CCC: $25.00
Published on Web 03/01/2003

Whereas the CD and EF sites in α—both high-affinity sites—are nearly indistinguishable in Ca^{2+}-binding assays (*16*, *17*), the two sites in *β* are distinctly nonequivalent (*18*, *19*). The *β* EF site is a typical high-affinity site; the CD site, by contrast, exhibits a low-affinity (or Ca^{2+}-specific) signature. A satisfactory explanation for the disparate behavior has proven elusive. There is increasing evidence, however, that structural features remote from the EF-hand motifs play a prominent role.

Permyakov et al. (*20*) have isolated the AB and CD-EF fragments from pike α parvalbumin and demonstrated that their reassociation is energetically linked to Ca^{2+} binding. Thus, the AB/CD-EF tertiary interaction could potentially modulate PV divalent ion-binding properties, a hypothesis we intend to explore using the rat α and *β* isoforms.

Preparatory to studying the AB/CD-EF interactions in rat α and *β*, we have examined the physical properties of their isolated CD-EF fragments. We herein present a detailed comparison of conformational stability, propensity for self-association, and Ca^{2+}-binding behavior. Thépault et al. (*21*) recently published the structure of α CD-EF and reported some preliminary physical data. This study complements their work and reveals intriguing differences between the two metal ion-binding domains.

MATERIALS AND METHODS

Cloning and Isolation of the β CD-EF Domain. Residues 38−108 of rat *β*-PV were amplified from the full-length coding sequence by PCR, using *Pfu* Turbo polymerase (Stratagene). The sense primer consisted of an Nde I site appended to the codons for residues 39−45. The anti-sense primer contained a BamH I site appended to the complementary sequence for residues 103 through the termination codon. The resulting PCR fragment was captured in pCR2.1 using the TOPO-TA cloning kit (Invitrogen) and subsequently—after confirming the sequence—cloned between the Nde I and the BamH I sites of pET11a (Novagen). This construct was then used to transform *Escherichia coli* BL21(DE3).

A 20-mL starter culture (LB broth supplemented with 100 *μ*g/mL of ampicillin and 1% D-glucose) was inoculated with a single colony and cultured overnight at 37 °C. The following morning, four 2-L Erlenmeyer flasks, containing 1.0 L of LB/ampicillin, were each inoculated with 5 mL of starter culture and incubated at 37 °C with shaking. When the A_{600} reached 0.5, IPTG was added to a final concentration of 1 mM, and incubation was continued at 37 °C for an additional 3 h. The cell paste, collected by centrifugation at 4 °C, was resuspended in four volumes of 20 mM Hepes-NaOH, pH 7.4, containing protease inhibitors (Complete Mini minus EDTA, Roche Diagnostic Labs) and stored at −20 °C.

Hen egg lysozyme was added to the thawed cell suspension to a final concentration of 0.2 mg/mL. After 15 min at 37 °C, the suspension was extruded through a French pressure cell chilled to 4 °C. Subsequent purification steps were performed at 4 °C. The crude lysate was clarified by centrifugation (27 000*g*, 30 min), then loaded onto DEAE-agarose (10 mL per liter of culture), preequilibrated with 20 mM Hepes-NaOH, pH 7.4. The column was developed with a 0−0.3 M NaCl gradient (10 bed volumes) prepared in the same buffer. Fractions containing the protein were identified by nondenaturing PAGE, combined, and concentrated to 5 mL in an Amicon ultrafiltration cell. This sample was then loaded onto Sephadex G-75 (3 × 80 cm), preequilibrated with 0.15 M NaCl, 0.025 M Hepes-NaOH, pH 7.4. Because the *β* CD-EF domain displays a characteristic absorbance spectrum, fractions of interest could be identified by UV spectroscopy. These were combined and stored at −20 °C. Each liter of culture yields approximately 40 mg of protein. On the basis of the A_{290}/A_{274} ratio, we conclude that the purity exceeds 98%. Protein concentration was measured spectrophotometrically, employing an extinction coefficient at 274 nm of 3260 M^{-1} cm^{-1}.

Cloning and Isolation of the α CD-EF Fragment. A comparable strategy was used to clone and express residues 39−109 of rat α-PV. However, isolation of α CD-EF was complicated by its much lower expression level. To remove impurities remaining after ion-exchange and gel-filtration, the α CD-EF fragment was subjected to nondenaturing preparative PAGE through 10% polyacrylamide, in a Model 491 Prep Cell (Bio-Rad Laboratories, Inc.). Material thus treated had negligible absorbance at 280 nm, indicating purity exceeding 98%. Prior to storage at −20 °C, the peptide was dialyzed into 0.15 M NaCl, 0.025 M Hepes-NaOH, pH 7.4. Protein concentrations were measured spectrophotometrically, employing an extinction coefficient at 258 nm of 900 M^{-1} cm^{-1}.

Because residue 38 of rat *β* is methionine, the translated sequence of the amplified product is identical to the wild-type protein, whether the initiating methionine is removed. On the other hand, residue 38 in rat α is lysine so that if the initiating methionine is retained, the sequence will contain a non-native residue at that position.

EDTA Agarose was used to extract residual divalent ions from protein solutions and buffers. The chelating matrix was prepared by adding 5.0 g of EDAC to 150 mL of aminohexyl agarose in 250 mL of 0.5 M EDTA, pH 6.0, then incubating at room temperature with constant agitation. After 1 h, a second 5.0-g aliquot of EDAC was added, and incubation was continued for another 4 h. The resulting material was washed with water and then with 10 mM Ca^{2+}, to remove excess EDTA. Prior to use, the gel was treated with dilute HCl (pH 2) to release bound divalent ions, then neutralized with 0.15 M NaCl, 0.025 M Hepes, pH 7.4. Aminohexyl agarose was prepared by activation with 1,4-butanediol-diglycidyl ether (*22*), followed by reaction with 1,6-diaminohexane at pH 13.

Analytical Ultracentrifugation studies were performed at 20 °C in a Beckman XL-I analytical ultracentrifuge. Prior to analysis, samples were dialyzed against the reference buffer: 0.15 M NaCl, 0.025 M Hepes-NaOH, pH 7.4, containing either 1.0 mM Ca^{2+} or 1.0 mM EDTA.

Equilibrium data were collected at 20 000 and 30 000 rpm, using charcoal-filled Epon six-channel centerpieces. The distributions of α and *β* CD-EF were monitored at 257 and 274 nm, respectively. Radial scans were obtained at 1-h intervals until successive scans were superimposable. Data were collected every 0.001 cm, averaging 20 readings at each step.

The three absorbance scans from each cell were extracted from the raw data with the Origin software (v.3.78, OriginLab) supplied with the instrument. Individual sedimentation

equilibrium experiments were analyzed by nonlinear least-squares (NLLS) in Origin, using fitting routines supplied by Beckman. Simultaneous, weighted analyses of multiple equilibrium data sets—i.e., global NLLS analysis—were performed with Origin (v.5.0), employing the fitting functions supplied below. The weighting factor for the *i*th data point equaled $1/(\sigma_i)^2$, where σ_i was the standard deviation of the absorbance reading for that point. A value of 0.73 cm^3/g was assumed for the partial specific volume; the solvent density was 1.001 g/cm^3.

Velocity data were acquired at 40 000 rpm, with charcoal-filled Epon dual-sector centerpieces. Absorbance data (257 nm for α CD-EF, 274 nm for β) were collected in the continuous mode. The distribution of sedimentation coefficients was analyzed by the time-derivative method (*23*), using software supplied with the instrument.

Isothermal Titration Calorimetry was performed in a MicroCal VP-ITC. Ca^{2+} solutions were standardized by calorimetric titration of EDTA solutions of known concentration. These were used in turn to standardize nitrilotriacetic acid solutions. Single experiments were analyzed with Origin fitting modules supplied with the instrument. Weighted global NLLS analyses were performed with a Fortran-based fitting program, written in-house, that utilizes the CUFIT algorithm from Bevington (*24*).

In this program, integrated injection heats are predicted by a two-step procedure. First, the free Ca^{2+} concentration is estimated by employing a bisection routine to solve the mass conservation equation, given the current vector of parameter values. Knowing the free ligand concentration (x), after the *j*th addition of titrant, the cumulative heat of binding (Q_j) can be calculated with eq 1:

$$Q_j = \sum_i Q_i = V_o M_T \sum_i \Delta H_i \frac{\beta_i x^i}{P} \qquad (1)$$

where Q_i is the heat associated with the *i*th form of the protein, V_o is the sample volume, M_T is the total macromolecule concentration, ΔH_i is the molar binding enthalpy for the *i*th form, β_i is the overall macroscopic binding constant for formation of the *i*th state, and P is the binding partition function. The corresponding heat associated with the *j*th addition of titrant, q_j, is equal to

$$q_j = Q_j - Q_{j-1} + \frac{dV_j}{V_o}\left[\frac{Q_j + Q_{j-1}}{2}\right] \qquad (2)$$

where Q_j and Q_{j-1} are the cumulative heats of binding after the j and $j - 1$ additions, respectively.

The third term on the right side of eq 2 corrects for the volume of solution displaced from the sample cell by the injection of titrant (dV_j). The binding models used to fit the α and β CD-EF data are described under Results.

Determination of Confidence Intervals. F statistics were used to generate 68% confidence intervals for the ITC fitting parameters. The *F* statistic—a ratio of two χ^2 values—allows comparison of two least-squares fits (*25*). If it exceeds a certain threshold, which depends on the number of fitting parameters and degrees of freedom, it is likely that the fit yielding the lower χ^2 value is superior.

Thus, after determining the minimum reduced χ^2 value, χ_r^2(min), we incremented the parameter of interest and fixed its value, then repeated the least-squares minimization, allowing the remaining parameters to float. This procedure yielded a new χ^2 value, χ_r^2(par), slightly larger than χ_r^2(min). This process was repeated until F_x, the ratio of the two χ^2 values, exceeded a specified limit. This limit is given by

$$F_x = \frac{\chi_r^2(\text{par})}{\chi_r^2(\text{min})} = 1 + \frac{p}{\nu}F(p,\nu,P) \qquad (3)$$

where p specifies the number of fitting parameters, ν is the degrees of freedom, P is the probability that the increase in χ_r^2 results from random errors (0.32 for the 68% confidence limit), and $F(p,\nu,P)$ is the corresponding F statistic. We used the $F(p,\nu,P)$ values tabulated by Lakowicz (*26*).

Circular Dichroism measurements were made with an Aviv 62DS circular dichroism spectrometer, using 0.1 or 1.0 cm cuvettes. Samples were dialyzed into 0.15 M NaCl, 0.01 M MOPS, pH 7.4, containing either Ca^{2+} (0.25−2.0 mM) or EDTA (1.0 mM). Thermal denaturation was monitored at 222 nm, acquiring data at 0.5° intervals between 10 and 90 °C.

Equilibrium Dialysis. Before use, Lucite dialysis blocks were soaked in 3% HNO_3, rinsed with deionized water and methanol, and allowed to dry. Dialysis tubing (Spectrapor 6, MWCO 2,000, Spectrum Laboratories) was soaked in 3% HNO_3 for 30 min with continuous agitation. After rinsing, the membrane was sandwiched between two dialysis blocks. Parafilm gaskets on both sides of the membrane prevented diffusion between adjacent wells.

The 0.60-mL samples of protein were added by syringe to the chambers on one side of the membrane. 0.60-mL aliquots of buffer (0.15 M NaCl, 0.025 M Hepes, pH 7.4) and Ca^{2+} were placed in the opposing chambers. Each of the buffer chambers also contained 0.5 μC_i of $^{45}Ca^{2+}$ (PerkinElmer Life Sciences). The dialysis blocks were incubated at room temperature (23 °C) in a humidified chamber with continuous agitation.

After 24 and 48 h, 100-μL aliquots were removed from protein and buffer wells, mixed with 10 mL of scintillation cocktail (Scinti-safe Econo 2, Fisher Scientific Co., Pittsburgh, PA), and counted. Identical levels of activity were observed at the two sampling times, confirming that equilibrium had been achieved. The resulting data were fit to a two-site Adair model:

$$\bar{X} = \frac{K_1[Ca^{2+}] + 2K_2K_1[Ca^{2+}]^2}{1 + K_1[Ca^{2+}] + K_2K_1[Ca^{2+}]^2} \qquad (4)$$

where $\bar{X}$ is the extent of binding, and K_1 and K_2 are the two macroscopic association constants.

Tb^{3+} Luminescence Measurements. Samples of β CD-EF, in 0.15 M NaCl, 0.025 M Hepes, pH 7.4, were titrated with Tb^{3+} at 25 °C. 2.0-μL aliquots of Tb^{3+} were added by syringe to 2.0-mL samples of protein, contained in a 4.0-mL cuvette equipped with a stir bar. Prior to beginning the titration, and after each titrant addition, luminescence was monitored (at 545 nm) in an SLM 8100 spectrofluorometer. The excitation wavelength of 282 nm falls well within the tyrosine absorption spectrum, so that bound Tb^{3+} ions were excited primarily

by resonance energy transfer from the phenolic side chain. The titrant—prepared by dissolving $TbCl_3$ (Sigma-Aldrich) in water—was standardized by titrating an EDTA solution of known concentration, using xylenol orange as the indicator.

The data were subject to global least-squares analysis using the following two-site model:

$$y = [\mathrm{CDEF}]_t\left(\frac{A_1K_1[\mathrm{Tb}^{3+}] + (A_1 + A_2)K_2K_1[\mathrm{Tb}^{3+}]^2}{1 + K_1[\mathrm{Tb}^{3+}] + K_2K_1[\mathrm{Tb}^{3+}]^2}\right) + BL \quad (5)$$

where y is the observed luminescence; $[\mathrm{CDEF}]_t$ is the total peptide concentration; $[\mathrm{Tb}^{3+}]$ is the free Tb^{3+} concentration; K_1 and K_2 are the two macroscopic Tb^{3+} binding constants; A_1 and A_2 are the signal amplitudes (normalized for concentration) associated with the first and second binding events, respectively; and *BL* is a baseline offset. The free Tb^{3+} concentration at each point is estimated by solving the relevant mass conservation equation, using the total Tb^{3+} concentration, the total peptide concentration, and the current estimates of the binding constants. This analysis was performed using Scientist (MicroMath Scientific Software). It can also be performed in Origin. However, the model must be entered as a LabTalk script, to solve for $[\mathrm{Tb}^{3+}]$.

RESULTS

Self-Association Studies. Preliminary sedimentation equilibrium studies suggested that the α and *β* CD-EF domains differed in their tendency to self-associate. This conclusion was confirmed by global least-squares analysis. Figure 1A,B displays data collected on α CD-EF at three peptide concentrations and two rotor speeds, in the presence of 1.0 mM EDTA or 1.0 mM Ca^{2+}, respectively. The data in Figure 1A were accommodated by an ideal, single-species model:

$$c_r = c_o \exp\left[\frac{M_r\omega^2(1 - \bar{\nu}\rho)}{2RT}(r^2 - r_o^2)\right] + BL \quad (6)$$

In eq 6, r is the radius; r_o is an arbitrary reference point; c_r and c_o are the macromolecule concentrations at r and r_o, respectively; M_r is the molecular weight; ω is the angular velocity of the rotor; $\bar{\nu}$ is the partial specific volume of the macromolecule; ρ is the solvent density; R is the gas constant; T is the absolute temperature; and *BL* represents a baseline offset to account for minor optical mismatch of the sample—solvent pairs. For this analysis, the global parameter M_r was fixed at the sequence-derived molecular weight (7700), and only the local parameters, c_o and *BL*, were varied. The solid lines through the data sets indicate the best weighted fit to the composite data set ($\chi_r^2 = 0.405$).

A minor improvement in χ_r^2 (to 0.361) was obtained by modeling these data with eq 7, which describes a reversible monomer−dimer equilibrium:

$$c_r = c_{m,o}\exp\left[\frac{M_r\omega^2(1 - \bar{\nu}\rho)}{2RT}(r^2 - r_o^2)\right] + c_{m,o}^2K_2\exp\left[\frac{2M_r\omega^2(1 - \bar{\nu}\rho)}{2RT}(r^2 - r_o^2)\right] + BL \quad (7)$$

In this expression, $c_{m,o}$ is the monomer concentration at r_o, and K_2 represents the association constant for dimer formation. The other symbols were defined above. For least-squares minimization, M_r was fixed at the sequence-derived value, and K_2 (global) was allowed to float. The local parameters, $c_{m,o}$ and *BL*, were likewise allowed to float. Although the reduction in χ_r^2 is marginally significant, the pattern of residuals observed at the highest loading concentration is consistent with self-association. In any event, the value of K_2 was just 240 M^{-1}, so that any tendency for Ca^{2+}-free α CD-EF to self-associate is extremely weak.

By contrast, satisfactory modeling of data collected on α CD-EF in the presence of 1.0 mM Ca^{2+} (Figure 1B) required inclusion of the dimerization term. The χ_r^2 value obtained with M_r fixed at 7780 and K_2 fixed at 1×10^{-20} M^{-1} was 1.74. However, when K_2 was permitted to float, χ_r^2 decreased significantly, to 0.42. The analysis returned a value of 3450 M^{-1} for K_2. Thus, α CD-EF exhibits a weak, but measurable, tendency to dimerize in the Ca^{2+}-bound form.

Comparable analyses of *β* CD-EF are displayed in Figure 1C,D. Panel C presents data collected in the presence of 1.0 mM EDTA. In contrast to the Ca^{2+}-free α domain, these data could not be modeled assuming a single species. However, eq 7 afforded a satisfactory fit. Fixing M_r at the sequence-derived value (8000) yielded an estimate of 2440 ± 180 M^{-1} for K_2, consistent with weak, but perceptible, self-association.

Figure 1D displays equilibrium data collected in the presence of 1.0 mM Ca^{2+}. These data were likewise modeled with eq 7, fixing M_r at 8080. The optimal fit, indicated by the solid lines through the data, yielded a value of 1.91(0.29) $\times 10^5$ M^{-1} for K_2.

Sedimentation Velocity. Samples of α CD-EF (■) and *β* CD-EF (○) were subjected to velocity analysis at 20 °C and 40 000 rpm, in Hepes-buffered saline containing 1.0 mM Ca^{2+}. Raw data from the latter stages of the run are displayed in Figure 2A. The *β* peptide displays a slightly larger average sedimentation coefficient.

Sedimentation coefficient distributions were examined by the Stafford time-derivative method (*23*) (Figure 2B). Whereas *β* CD-EF (○) yields a peak in the g(s*) plot, the α fragment (■) does not. These findings are consistent with the sedimentation equilibrium data presented above—i.e., *β* being predominantly dimeric under these conditions and α being a mixture of monomer (predominantly) and dimer.

Stability Studies. The relative thermal stabilities of the α and *β* CD-EF peptides were examined by far-UV circular dichroism (CD) measurements. Thermal melts were performed at several Ca^{2+} concentrations: 0, 0.25, 0.5, and 1.0 mM for α-CDEF and 0, 0.5, 1.0, and 2.0 mM for *β* CD-EF. The resulting data are displayed in Figure 3, panels A and B. In the absence of Ca^{2+}, the CD signals are weak, and neither peptide exhibits a sigmoidal transition, in agreement with the previously published data of Thépault et al. (*21*) for the α CD-EF domain. The α CD-EF domain is substantially more stable than the *β* fragment over the entire range of Ca^{2+} examined, most likely a reflection of its higher affinity for the ion (vide infra).

After determining the apparent T_m for each peptide at each Ca^{2+} concentration, the samples were cooled, then reheated. In every case, the two scans were superimposable, indicating that the unfolding processes are reversible. The α and *β* CD-

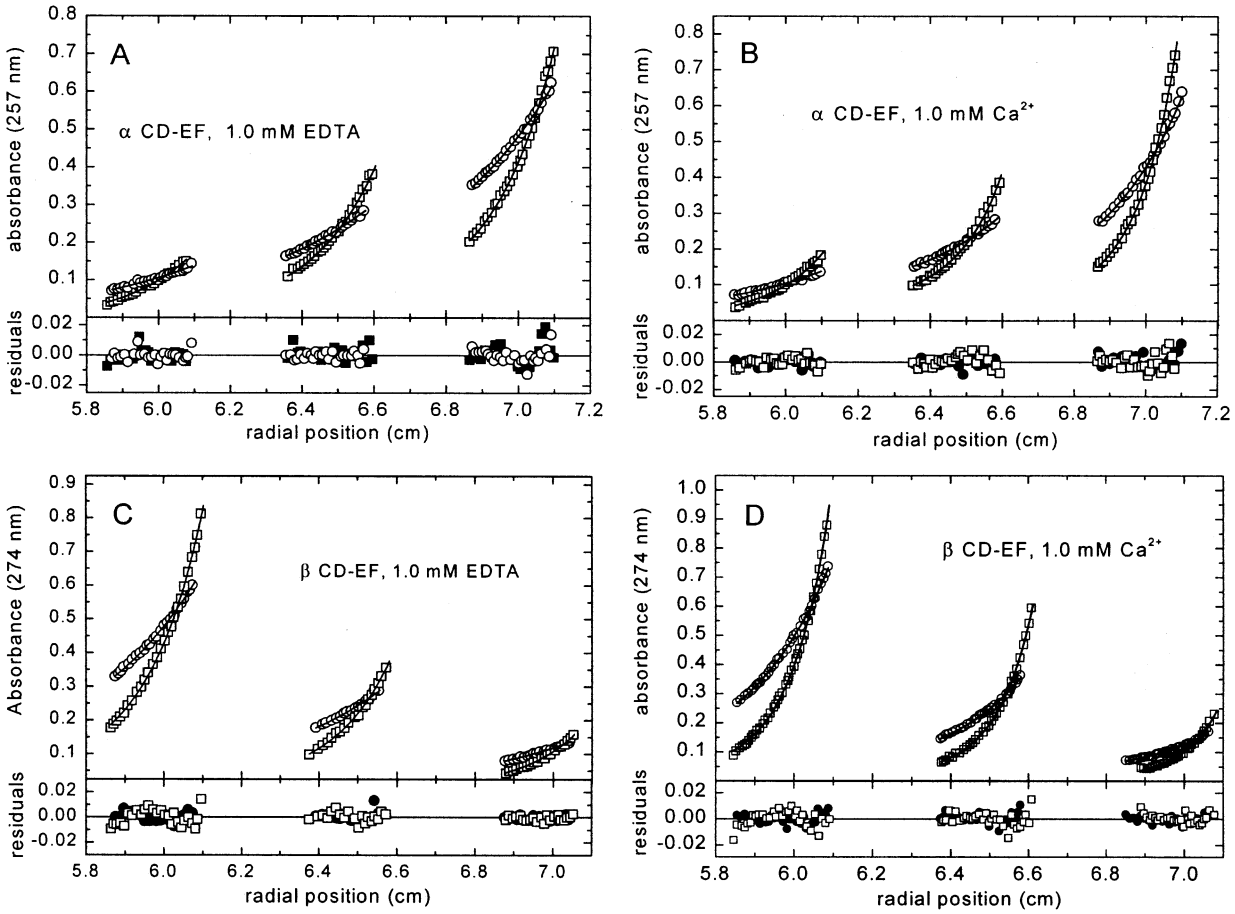

FIGURE 1: Global sedimentation equilibrium analyses. Samples were centrifuged at 20 000 (○) and 30 000 rpm (□) (A). α CD-EF in buffer containing 1.0 mM EDTA. From left to right, the loading concentrations were 125, 250, and 500 μM. (B) α CD-EF (110, 220, 450 μM) in buffer containing 1.0 mM Ca^{2+}. (C) β CD-EF (loading concentrations of 150, 75, and 38 μM) in buffer plus 1.0 mM EDTA. (D) β CD-EF (170, 85, and 42 μM loading concentrations) in buffer plus 1.0 mM Ca^{2+}. Sedimentation was monitored at 257 nm (α) or 274 nm (β). For clarity, only subsets of the data are displayed, and select sets of residuals are represented by filled symbols.

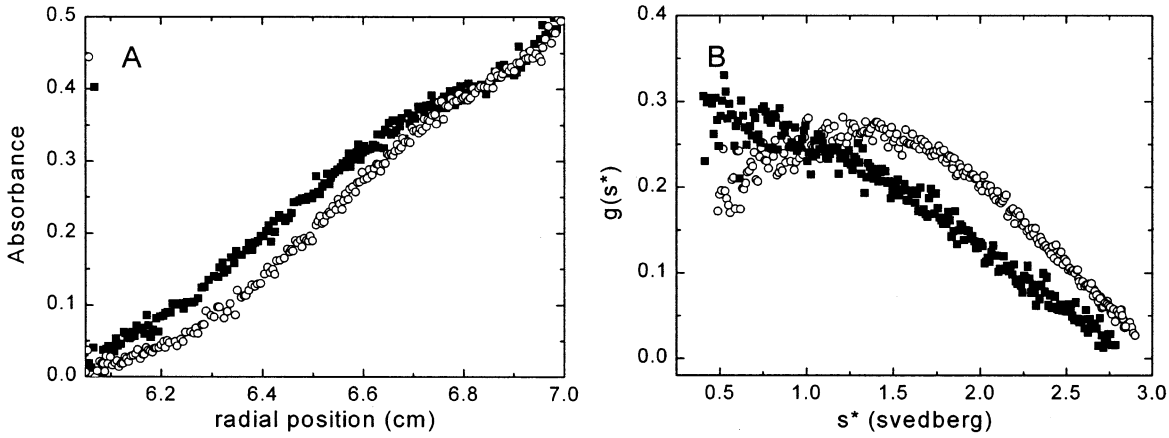

FIGURE 2: Sedimentation velocity analysis of α and β CD-EF. Samples of the α (■) and β (○) peptides were sedimented in 0.15 M NaCl, 0.025 M Hepes, pH 7.40, at 40 000 rpm and 20 °C. The initial loading concentration was 420 μM for α and 160 μM for β. (A) Raw data 487 min into the run. (B) The distribution of sedimentation coefficients in the two samples.

EF thermal denaturation data were fit to the following equation:

$$y = \left[\frac{(y_f + m_f T) + (y_u + m_u x)\exp[(\Delta H_u/RT)((T - T_m)/T_m)]}{1 + \exp[(\Delta H_u/RT)((T - T_m)/T_m)]}\right] \quad (8)$$

where y is the raw ellipticity signal; m_f and y_f, and m_u and y_u represent the slope and intercept, respectively, for the pre- and post-transition baselines; ΔH_u is the apparent, or van't Hoff, enthalpy for denaturation; and T_m is the absolute melting temperature (*27*). The T_m and ΔH_u values for the various thermal denaturation experiments have been compiled in Table 1.

We also examined the stabilities of the α and β CD-EF fragments as a function of peptide concentration, at a free

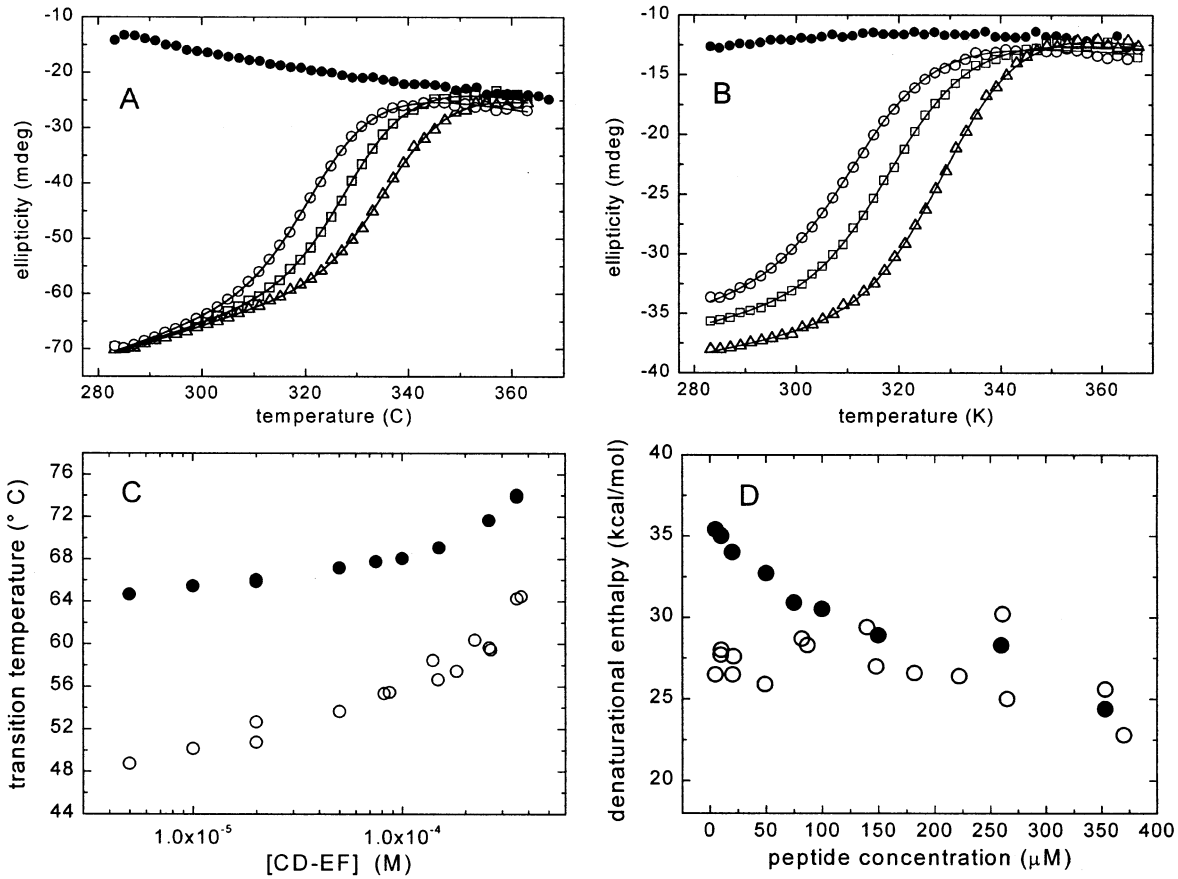

FIGURE 3: Thermal stabilities of α and β CD-EF. (A) Thermal stability of 5 μM α CD-EF in 1.0 mM EDTA (●) and in the presence of 0.25 mM (○), 0.5 mM (□), and 1.0 mM (△) Ca^{2+}. (B) Stability of 5 μM β CD-EF in 1.0 mM EDTA (●) and in the presence of 0.5 mM (○), 1.0 mM (□), and 2.0 mM (△) Ca^{2+}. (C) Melting temperatures of α (●) and β CD-EF (○) as a function of peptide concentration, in 1.0 mM Ca^{2+}. (D) Apparent denaturational enthalpies of α (●) and β CD-EF (○) as a function of peptide concentration, in 1.0 mM Ca^{2+}.

Table 1: Thermal Stabilities of Rat α and β CD-EF Fragments

peptide	[peptide] (M)	[Ca^{2+}] (M)	T_m (°C)	ΔH_u (kcal/mol)
α CD-EF	5.0×10^{-6}	2.5×10^{-4}	49.95	31.7
	5×10^{-6}	5.0×10^{-4}	56.75	34.0
	5×10^{-6}	1.0×10^{-3}	64.65	35.4
	1.0×10^{-5}	1.0×10^{-3}	65.45	35.0
	2.0×10^{-5}	1.0×10^{-3}	65.95	34.0
	5.0×10^{-5}	1.0×10^{-3}	67.15	32.7
	7.5×10^{-5}	1.0×10^{-3}	67.75	30.9
	1.0×10^{-4}	1.0×10^{-3}	68.05	30.5
	1.5×10^{-4}	1.0×10^{-3}	69.05	28.9
	2.6×10^{-6}	1.0×10^{-3}	71.65	28.3
	3.53×10^{-4}	1.0×10^{-3}	73.95	24.4
β CD-EF	4.8×10^{-6}	5.0×10^{-4}	40.15	24.7
	4.8×10^{-6}	1.0×10^{-3}	48.75	26.5
	4.8×10^{-6}	2.0×10^{-3}	57.55	27.7
	9.7×10^{-6}	1.0×10^{-3}	50.15	28.0
	1.0×10^{-5}	1.0×10^{-3}	50.15	26.5
	2.0×10^{-5}	1.0×10^{-3}	50.75	27.6
	2.1×10^{-5}	1.0×10^{-3}	52.65	25.9
	4.9×10^{-5}	1.0×10^{-3}	53.65	28.7
	8.2×10^{-5}	1.0×10^{-3}	55.35	28.3
	8.7×10^{-5}	1.0×10^{-3}	55.45	29.4
	1.4×10^{-4}	1.0×10^{-3}	58.45	27.0
	1.48×10^{-4}	1.0×10^{-3}	56.65	26.6
	1.82×10^{-4}	1.0×10^{-3}	57.45	26.4
	2.22×10^{-4}	1.0×10^{-3}	60.35	30.2
	2.61×10^{-4}	1.0×10^{-3}	59.65	25.0
	2.65×10^{-4}	1.0×10^{-3}	59.45	25.6
	3.53×10^{-4}	1.0×10^{-3}	64.25	22.8
	3.70×10^{-4}	1.0×10^{-3}	64.45	23.4

Ca^{2+} concentration of 1.0 mM (Figure 3C,D). The T_m for β CD-EF displays greater concentration-dependence, consistent with its greater tendency to self-associate. However, at sufficiently high concentrations, the T_m for the α fragment also becomes concentration dependent.

The apparent enthalpies of unfolding for both peptides are small, consistent with their diminutive size. Notice that the values measured for β CD-EF at low peptide concentration are significantly smaller than those observed with the α peptide (Table 1, Figure 3D). Moreover, the denaturational enthalpy for β is independent of transition temperature (or peptide concentration), within the precision of the analysis. By contrast, the apparent enthalpy of denaturation for α decreases perceptibly with increasing transition temperature, approaching that of β at high peptide concentrations.

Ca^{2+}-Binding Properties of Rat α. Raw Ca^{2+}-binding data for α CD-EF are displayed in Figure 4A, and the corresponding integrated data are displayed in Figure 4B (○). α CD-EF binds two Ca^{2+}. Thus, the integrated injection heats (q_j) were fit to eq 2, employing this general expression for Q_j, the cumulative heat of binding after the jth addition:

$$Q_j = M_t V_o \left[\frac{\Delta H_1 K_1 [Ca^{2+}] + (\Delta H_1 + \Delta H_2)[Ca^{2+}]^2}{1 + K_1 [Ca^{2+}] + K_2 K_1 [Ca^{2+}]^2} \right] \quad (9)$$

In this equation, M_t is the total protein concentration, V_o is the sample cell volume, ΔH_1 and ΔH_2 are the enthalpies associated with the first and second binding events, and K_1 and K_2 are the corresponding binding constants.

Strong correlation between ΔH_1 and ΔH_2 ($R_{ij} = 0.99$) frustrated initial efforts to uniquely fit this system. Reasoning

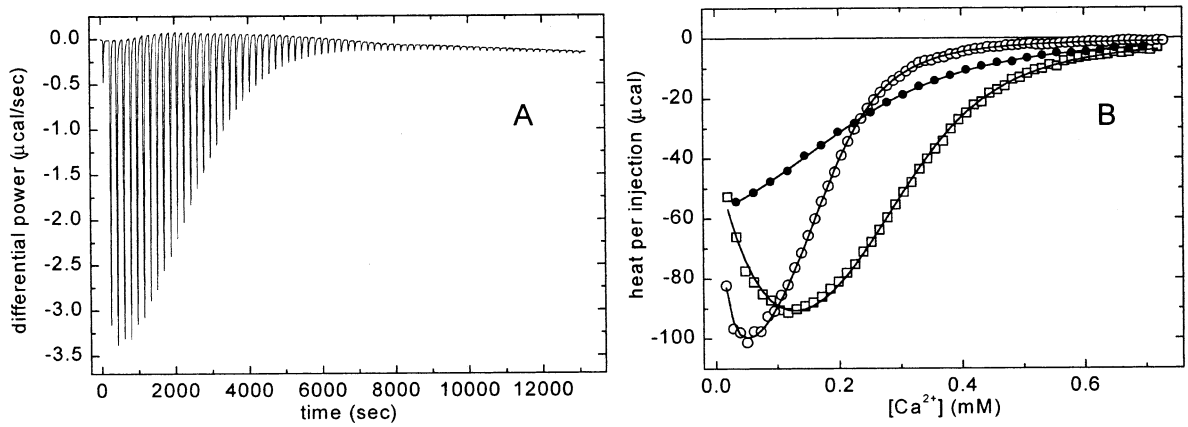

FIGURE 4: ITC analysis of Ca^{2+} binding by α CD-EF. (A) Representative raw data for titration of 60 μM peptide with 2.0 mM Ca^{2+}. (B) Global analysis of Ca^{2+} binding by α CD-EF. Titration of 0.25 mM NTA (●); titration of 60 μM CD-EF (○); and titration of 60 μM CD-EF, in the presence of 0.125 mM NTA (□).

Table 2: Calcium-Binding Properties of Rat α and β CD-EF Domains

		Binding Constants			Binding Enthalpies		
peptide	method	param	value (M^{-1})	confidence interval	param	value (kcal/mol)	confidence interval
α CD-EF	ITC	K_1	3.67×10^3	3.60, 3.73	ΔH_1	−17.2	−17.4, −17.1
		K_2	8.58×10^4	8.51, 8.83	ΔH_2	−4.05	−4.27, −3.93
β CD-EF	dialysis	K_1	4.25×10^3	3.20, 5.30			
		K_2	6.07×10^3	4.07, 8.07			
	ITC	K_D	2.67×10^3	2.27, 3.18	ΔH_D	+5.60	5.39, 5.95
		K_1	3.61×10^3	3.49, 3.74	ΔH_1	+2.12	1.97, 2.24
		K_{1D}	1.36×10^4	1.29, 1.41	ΔH_{1D}	−15.7	−17.0, −15.5
		K_{D2}	6.65×10^7	4.94, 8.76	ΔH_{D2}	−17.1	−19.0, −16.4
		K_{D4}	1.63×10^8	1.48, 1.77	ΔH_{D4}	+1.76	1.66, 1.94

that the presence of a competing ligand might break the degeneracy, we performed a titration in the presence of 0.125 mM nitrilotriacetic acid (NTA). Under our experimental conditions, NTA binds a single equivalent of Ca^{2+} with an association constant of 11 700 M^{-1} and a binding enthalpy of −1.96 kcal/mol (Figure 4B, ●).

The α CD-EF data sets acquired in the absence (Figure 4B, ○) and presence (Figure 4B, □) of NTA were analyzed simultaneously. For data gathered in the presence of NTA, eq 9 was replaced by this amended expression for the cumulative heat of binding:

$$Q_j = I_t V_o \left[\frac{\Delta H_I K_I [Ca^{2+}]}{1 + K_I [Ca^{2+}]}\right] + M_t V_o \left[\frac{\Delta H_1 K_1 [Ca^{2+}] + (\Delta H_1 + \Delta H_2)[Ca^{2+}]^2}{1 + K_1 [Ca^{2+}] + K_2 K_1 [Ca^{2+}]^2}\right] \quad (10)$$

where I_t is the total NTA concentration, and ΔH_I and K_I are the binding enthalpy and Ca^{2+} association constant, respectively, for the competitor.

This strategy yielded a unique set of parameter values, displayed in Table 2 along with the 68% confidence limits. The solid lines through the data in Figure 4B represent the best least-squares fit. With K_1 and K_2 values of $3.7(0.1) \times 10^3$ M^{-1} and $8.6(0.2) \times 10^4$ M^{-1}, respectively, Ca^{2+} binding to α CD-EF is evidently strongly cooperative. It is also highly exothermic, with the bulk of heat release accompanying ligation of the first ion.

Ca^{2+}- and Tb^{3+}-Binding Properties of Rat β. Initial ITC experiments on β CD-EF (e.g., Figure 5A) cast uncertainty on the Ca^{2+}-binding stoichiometry. Satisfactory modeling of the data with eqs 2 and 9 required an input value for M_t exactly one-half the monomer concentration (Figure 5B, solid line). In view of the sedimentation equilibrium data for the peptide, this result might have signified that β CD-EF functioned as a dimer with just one functional binding site per subunit.

$^{45}Ca^{2+}$ equilibrium dialysis was performed to obtain an unequivocal estimate of the stoichiometry. Figure 6 displays data from two separate experiments, plotted as molar equivalents of Ca^{2+} bound (per monomer) vs $[Ca^{2+}]$. The best least-squares fit to a two-site Adair model (eq 4) yields an apparent stoichiometry of 2.01 Ca^{2+} per monomer—evidence that the CD and EF sites of β both retain the capacity to bind Ca^{2+} in the isolated CD-EF fragment. The accompanying estimates for K_1 and K_2—$4.2(1.0) \times 10^3$ M^{-1} and $6.1(2.0) \times 10^3$ M^{-1}, respectively—indicate that Ca^{2+} binding is positively cooperative.

Reassured that β CD-EF binds two equivalents of Ca^{2+}, we resumed analysis of the ITC data. Experiments were performed at several β CD-EF concentrations: 58 μM (▽,◇), 116 μM (□), and 250 μM (○). An additional titration (58 μM β CD-EF, △) was conducted in the presence of NTA. The integrated data for these five experiments are presented in Figure 7. Our objective was to develop a minimal model capable of accommodating all of these data.

The relative complexity of this system—the microstates for which are enumerated in Figure 8A—necessitated several assumptions. First, we assumed that—at the concentrations we were employing—any fully bound peptide is dimeric, eliminating species 4. Additionally, in full-length rat β-PV,

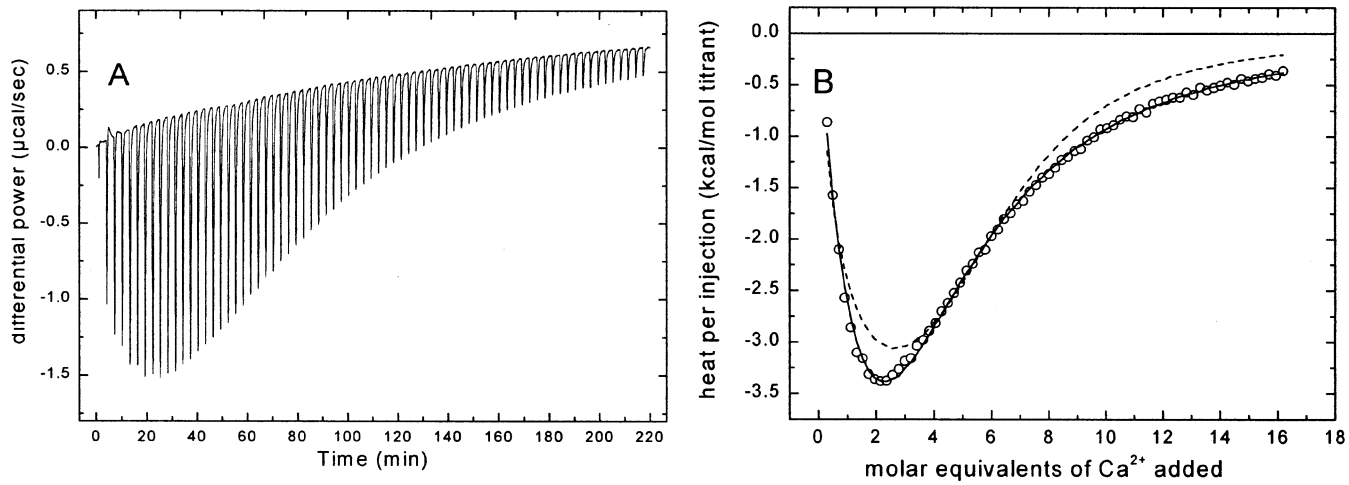

FIGURE 5: Initial ITC analysis of Ca^{2+} binding by β-CDEF. (A) Representative raw data for titration of 150 μM peptide with 2.0 mM Ca^{2+}. (B) Integrated data from panel A, with best least-squares fits to a two-site Adair equation, assuming peptide concentrations of 150 μM (dashed line) or 75 μM (solid line).

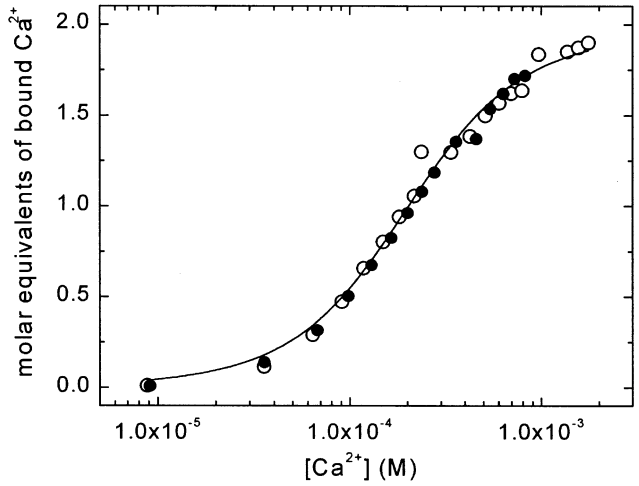

FIGURE 6: Analysis of Ca^{2+} binding by β CD-EF by equilibrium dialysis. The 0.60-mL samples of 0.24 mM peptide were dialyzed against 0.60 mL of buffer containing 0.5 μC_i of $^{45}Ca^{2+}$ and increasing amounts of nonradioactive Ca^{2+}, as described in Materials and Methods. Open and filled symbols represent data from two separate experiments.

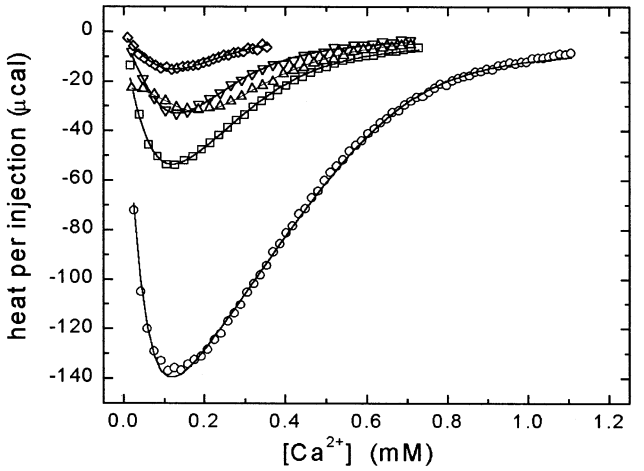

FIGURE 7: Global analysis of ITC data for binding of Ca^{2+} by β CD-EF. The composite data set employed for analysis included these titrations: 2.0 mM Ca^{2+} vs 58 μM peptide ($\diamond$); 4.0 mM Ca^{2+} vs 58 μM peptide ($\triangledown$); 4.0 mM Ca^{2+} vs 58 μM peptide in the presence of 0.125 mM NTA ($\triangle$); 4.0 mM Ca^{2+} vs 116 μM peptide ($\square$); and 6.0 mM Ca^{2+} vs 250 μM peptide ($\bigcirc$). Solid lines reflect the best least-squares fit to the data.

the CD site Ca^{2+} affinity is roughly 20 times lower than the EF site affinity. If this preference is maintained in the isolated CD-EF fragment, those species in which ligation occurs preferentially at the CD site will not be significantly populated—eliminating 2, 6, 8, 9, 11, and 12. Finally, we assumed that binding is highly cooperative, so that singly and triply bound species are negligibly populated, eliminating the need to consider species 7 and 13. We are left with the minimal binding scheme depicted in Figure 8B, the derivation of which is briefly outlined in the appendix.

We initially assumed that all binding proceeded through the singly ligated monomeric state, which subsequently dimerized. Although satisfactory at low peptide concentrations, this model did not accommodate intermediate- and high-concentration data. Recall that our sedimentation analysis indicated that Ca^{2+}-free β CD-EF self-associates weakly. Presumably, at 116 and 250 μM, the apo-dimer form is significantly populated, permitting binding to occur via the alternative pathway.

In this alternative pathway, binding of the first two ions to the apo-protein is assumed to be highly cooperative, governed by a single binding constant K_{D2}. We also explored a model in which binding of the two ions occurred sequentially. The latter was discarded for several reasons. First, the improvement in χ_r^2 was not significant. Moreover, the estimate obtained for the second binding constant was invariably much larger than the first, indicative of highly cooperative binding. Finally, during the fitting process, the magnitudes of the two binding enthalpies invariably became unrealistically large—one negative, one positive.

Occupation of the remaining two sites in the dimer, governed by the K_{D4} binding constant, is likewise assumed to be simultaneous. Again, we explored a model in which the binding events occurred sequentially but discarded it for reasons similar to those given above.

Although the minimal model shown in Figure 8B includes 10 parameters, only eight are independent. The other two are constrained by thermodynamic additivity. The solid lines in Figure 7 indicate the best fit to the data. The optimal

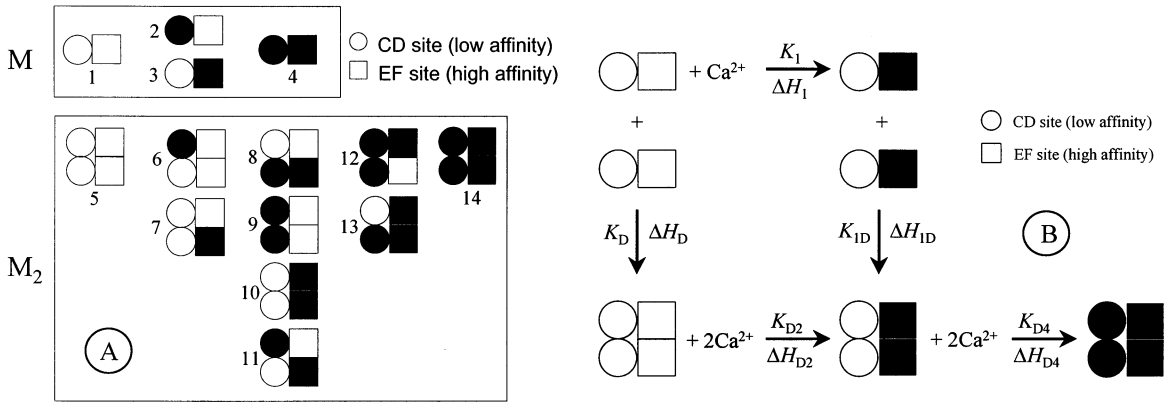

FIGURE 8: Modeling the β CD-EF ITC data. (A) Compilation of the relevant microstates. The CD site is symbolized by a circle, the EF site by a square. Open symbols represent vacant sites, filled symbols occupied sites. (B) Minimal model used to accommodate the ITC data presented in Figure 7.

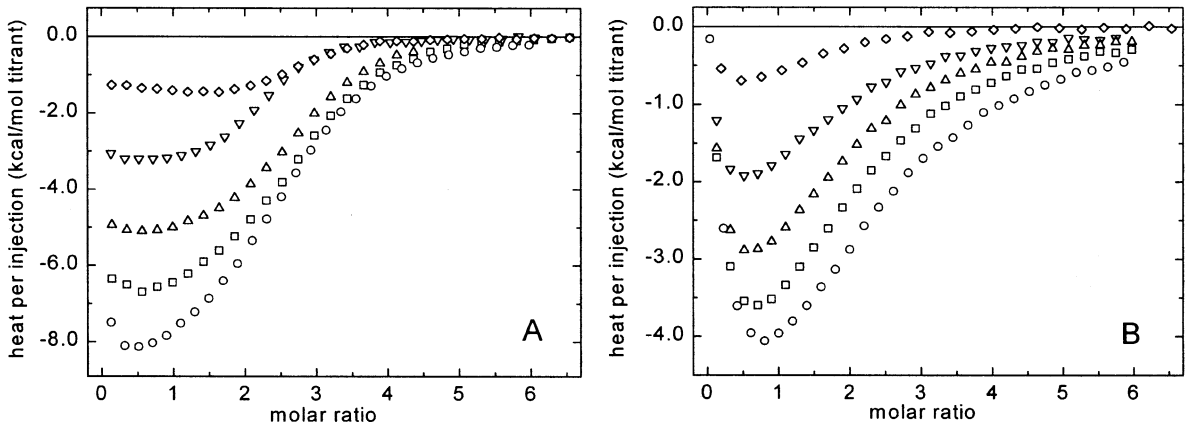

FIGURE 9: Temperature dependence of Ca^{2+} binding. Identical peptide samples were titrated with Ca^{2+} at temperatures ranging from 5 to 25 °C. The integrated data are displayed above. 5 (◇), 10 (▽), 15 (△), 20 (□), and 25 (○) °C. (A) 137 μM α CD-EF. (B) 150 μM β CD-EF.

parameter values, and the 68% confidence limits, are presented in Table 2.

Ca^{2+} binding was also examined as a function of temperature. For both peptides, the enthalpy was strongly temperature-dependent, becoming increasingly exothermic as the temperature is raised (Figure 9). This result is expected because binding is linked to folding and therefore accompanied by burial of substantial apolar surface area.

Tb^{3+} Binding. To further probe the metal ion-binding properties of β CD-EF, we examined its interaction with Tb^{3+}, an oft-used spectroscopic probe of EF-hand proteins. Sedimentation equilibrium analyses indicated that the peptide was exclusively dimeric in the presence of 0.5 mM Tb^{3+}. All six data sets could be fit simultaneously with eq 6, assuming the presence of a single 16 kDa species (Figure 10A).

Binding of the lanthanide was monitored by fluorescence—exciting the ion at 282 nm. At this wavelength, excitation of the bound ion occurs primarily via energy transfer from Tyr-57 and Tyr-65. Signal intensity (at 545 nm) is plotted versus total Tb^{3+} concentration in Figure 10B for experiments conducted at nominal peptide concentrations of 5, 10, and 20 nM. These curves plateau at Tb^{3+} concentrations consistent with a Tb^{3+}/protein stoichiometry of 2.0. The data were analyzed globally using eq 5, as described in Materials and Methods.

The best global fit to the composite data, indicated by the solid lines, yielded K_1 and K_2 values of $1.1(0.6) \times 10^6$ and $1.3(0.3) \times 10^6$ M^{-1}, respectively, and a signal amplitude ratio (A_2/A_1) of 3.8. The magnitudes of the two binding constants indicate that Tb^{3+} binding occurs with positive macroscopic cooperativity.

When 20 μM β CD-EF is titrated with Tb^{3+} in the presence of 5.0 mM Ca^{2+}, the binding curve is displaced to higher concentration because of competition by the divalent ion. Under these conditions, least-squares analysis of these data yields $K_1 = 5.6\ (1.4) \times 10^5$ M^{-1} and $K_2 = 1.0\ (0.2) \times 10^5$ M^{-1}. Thus, K_1 decreases by 50% and K_2 by a factor of 13.

DISCUSSION

Relative to rat α, rat β parvalbumin exhibits low affinity for Ca^{2+} and Mg^{2+}. In Hepes-buffered saline, the association constants for the EF and CD sites are reduced by factors of 5 and 100, respectively. There is substantial evidence that this attenuation results largely from structural determinants outside the binding pockets.

Modest Impact of Local Sequence Nonidentities. Investigators have noted that $\beta \rightarrow \alpha$ substitutions within the CD binding loop have minimal impact on Ca^{2+} affinity (*18*, *29*−*31*). Consider the D59E mutation. The presence of aspartate at the $-x$ position is unique to the mammalian β isoform; all other parvalbumins employ glutamate. Whereas the glutamyl carboxylate directly coordinates the bound Ca^{2+}, the shorter aspartyl side chain coordinates indirectly, via an intervening water molecule. Despite the major difference in

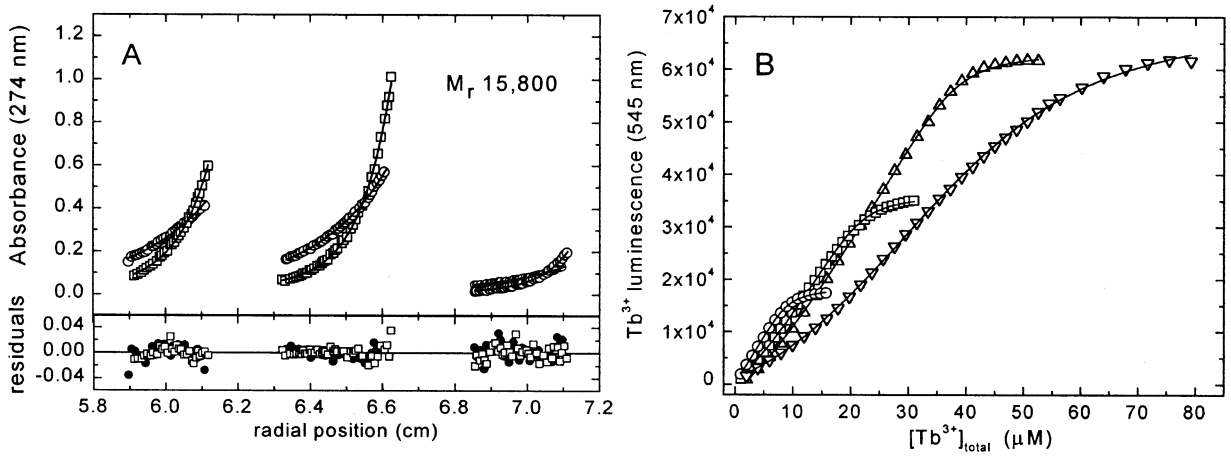

FIGURE 10: Interaction of β CD-EF with Tb^{3+}. (A) Samples of β CD-EF were centrifuged to equilibrium at 20 000 and 30 000 rpm, in 0.15 M NaCl, 0.025 M Hepes-NaOH, pH 7.4, containing 0.5 mM Tb^{3+}. Nominal loading concentrations, from left to right, were 60, 120, and 30 μM. The composite data set was analyzed globally, assuming a single species. (B) Titration of β CD-EF with Tb^{3+}. Samples of β CD-EF were titrated with Tb^{3+} in Hepes-buffered saline, pH 7.4. Following each addition, luminescence was measured at 545 nm (λ_{ex} = 282 nm). 1.0 mM Tb^{3+} vs 5 μM peptide (○); 1.0 mM Tb^{3+} vs 10 μM peptide (□); 2.0 mM Tb^{3+} vs 20 μM peptide (△); 2.0 mM Tb^{3+} vs 20 μM peptide, in the presence of 5.0 mM Ca^{2+} (▽). Raw fluorescence data, corrected for dilution, are plotted vs total Tb^{3+} concentration.

ligation, replacement of Asp-59 in rat β by glutamate improves the standard free energy for Ca^{2+} binding by just 0.2 kcal/mol (*18*).

Context-Dependent Performance of the CD and EF Binding Arrays. The parvalbumin CD and EF sites differ in both a local and a global sense. Locally, the ligand arrays differ at $+z$ and $-x$—serine and aspartate/glutamate in the CD site, aspartate and glycine in the EF site. The two sites also differ with respect to placement within the protein. Whereas the EF site is proximal to the C-terminus, the CD site is positioned in the middle of the sequence. This global context can supersede the influence of the local sequence differences. For example, when the (high-affinity) EF-site binding array is placed in the context of the β CD loop, it acquires the low-affinity signature characteristic of the wild-type CD site (*32*).

^{15}N NMR Relaxation Measurements. We recently performed ^{15}N relaxation measurements on Ca^{2+}-bound and -free rat β and analyzed the data using the standard Lipari−Szabo model-free formalism (*33*). Unexpectedly, the AB domain and, indeed, the D/E region of the protein appear to be more rigid in the Ca^{2+}-free state. This result suggests that Ca^{2+}-binding provokes a conformational alteration in these regions. Conceivably, the energetic cost of that alteration could contribute to the attenuated Ca^{2+} affinity displayed by β.

Evidence for Thermodynamic Linkage between Ca^{2+} Binding and AB/CD-EF Association. Permyakov et al. (*20*) presented evidence that association of the AB and CD-EF domains is linked to Ca^{2+} binding. They treated pike parvalbumin III with CNBr (which cleaves the polypeptide chain after Met-37), isolated the resulting fragments, then studied the energetics of their reassociation by fluorescence. A higher concentration of EGTA was required to extract Ca^{2+} from the CD-EF fragment in the presence of the AB domain. Conversely, when the CD-EF fragment was titrated with AB, an increase in fluorescence—indicative of complexation—was observed only when Ca^{2+} was present.

Given these data and the cumulative evidence that remote structural features influence parvalbumin divalent ion affinity, it is likely that the AB/CD-EF tertiary interaction is a significant determinant of PV metal ion-binding behavior. We plan to test this hypothesis using the rat α and β isoforms. Prior to initiating this analysis, we have compared the physical and divalent ion-binding properties of the isolated CD-EF fragments. Relative to the β peptide, α CD-EF displays a reduced tendency to self-associate, greater conformational stability, and higher Ca^{2+} affinity.

Self-Association. α CD-EF displays a weak tendency to dimerize. The Ca^{2+}-free peptide is monomeric, and in 1.0 mM Ca^{2+}, K_2 is only 3450 ± 200 M^{-1}. The β peptide shows a markedly greater propensity for dimerization. In 1.0 mM EDTA, K_2 = 2440 ± 180 M^{-1}. In 1.0 mM Ca^{2+}, it increases to 1.91(±0.29) × 10^5 M^{-1}.

Full-length rat α and β parvalbumins show no inclination to self-associate, even at millimolar concentrations. The tendency for the isolated CD-EF fragments to dimerize is undoubtedly due to exposure of apolar surface area that is sequestered—by association with the AB domain—in the intact proteins. Given that the α and β peptides should expose comparable apolar surface areas, their disparate self-association behavior is quite unexpected. The greater tendency for β to dimerize is especially counter-intuitive—considering its higher net charge and lower Ca^{2+} affinity—and suggests that the Ca^{2+}-bound α and β CD-EF fragments differ significantly in conformation (vide infra). This difference could significantly impact the divalent ion-binding properties of the full-length proteins.

Conformational Stability. Thermal denaturation of α and β CD-EF was monitored by CD. In the presence of EDTA, they exhibit minimal ellipticity, and neither undergoes a sigmoidal transition—suggesting that the peptides are largely disordered in the Ca^{2+}-free state. This behavior contrasts with other well-studied EF-hand domains e.g., calbindin D_{9k} (*34*), the isolated N- and C-domains of calmodulin (*35*, *36*), and the isolated N- and C-terminal domain of skeletal troponin C (*37*). Contrasting the parvalbumin CD-EF domain with calbindin, Thépault et al. (*21*) observed that the region linking the parvalbumin CD and EF sites is devoid of hydrophobic residues. By contrast, Leu-39 and Leu-40 anchor the calbindin linker region to the hydrophobic core, imparting stability, and Phe-36 interacts with Ile-73, near the C-terminus.

In the presence of Ca^{2+}, reversible cooperative denaturation is observed for both peptides. As expected, the apparent T_m is strongly dependent on Ca^{2+} concentration. Under all conditions examined, α CD-EF exhibits greater stability, consistent with its higher Ca^{2+} affinity.

The T_m for β CD-EF exhibits a strong dependence on peptide concentration. Although the concentration-dependence of T_m is less pronounced for the α peptide, there is distinct curvature at the highest peptide concentrations examined.

The apparent enthalpy of unfolding ($\Delta H_{u,app}$) is smaller for β CD-EF than for α. And whereas $\Delta H_{u,app}$ for β is essentially independent of peptide concentration, $\Delta H_{u,app}$ for α decreases with increasing concentration (Figure 3D). These differences probably reflect the disparate self-association tendencies of the two peptides.

Our ITC analysis of Ca^{2+} binding to β CD-EF (vide infra) indicates that the dimerization event (independent of folding) is endothermic. Thus, the obligatory dissociation that must accompany denaturation will be exothermic, reducing the magnitude of the (endothermic) denaturational enthalpy. The temperature-dependence of the apparent enthalpy of denaturation under these circumstances is described by

$$\Delta H_{u,app}(T) = [\Delta H_u(T_o) + \Delta C_{p,u}(T - T_o)] - \alpha_D[\Delta H_D(T_o) + \Delta C_{p,D}(T - T_o)] \quad (11)$$

where ΔH_u and $\Delta H_{u,app}$ are the true and apparent enthalpies of unfolding, respectively, for the monomer; ΔH_D is the enthalpy of dimerization; $\Delta C_{p,u}$ is the change in heat capacity of the monomeric peptide upon unfolding; $\Delta C_{p,D}$ is the change in heat capacity that accompanies dimerization; α_D is the fraction of the peptide in the dimeric state; T_o is an arbitrary reference temperature; and T is the temperature of interest. We expect $\Delta C_{p,u}$ to be positive because of increased solvent exposure of apolar side-chains. Conversely, we anticipate that $\Delta C_{p,D}$ should be negative because dimerization reduces accessible apolar surface area. However, the diminutive size of the CD-EF peptides also leads us to expect both quantities to be small, so that ΔH_u should display a minimal intrinsic temperature-dependence.

α_D will be approximately 1.0 for β CD-EF, over the range of concentrations examined, because of the peptide's relatively strong tendency to self-associate. Thus, the correction term in eq 11 will be significant—substantially lowering $\Delta H_{u,app}$—and essentially concentration-independent. By contrast, at the lowest α CD-EF concentration, α_D is small, and the apparent denaturational enthalpy approaches the true value. However, as the α CD-EF concentration is raised, α_D increases, causing the correction term in eq 11 to become progressively larger. In consequence, $\Delta H_{u,app}$ decreases significantly with concentration.

Metal Ion-Binding Properties. *α CD-EF*. The binding of Ca^{2+} to α CD-EF is highly cooperative, with $K_1 = 3.7 \times 10^3\ M^{-1}$ and $K_2 = 8.6 \times 10^4\ M^{-1}$ (overall $\Delta G^{\circ\prime} = -11.5$ kcal/mol). The first Ca^{2+}-binding event is strongly exothermic (−17.2 kcal/mol) because it is linked to folding and the concomitant establishment of myriad noncovalent interactions. The affinity is reduced, however, because a substantial fraction of the intrinsic binding free energy is used to promote the structural rearrangement. Although the second ion pays a smaller energetic penalty, binding to a more structured site, the magnitude of the binding enthalpy (−4.0 kcal/mol) is also reduced. Under the conditions employed for this analysis, dimerization of α CD-EF is negligible.

β CD-EF. Equilibrium dialysis experiments (Figure 6) yield apparent macroscopic binding constants of 4.2×10^3 and $6.1 \times 10^3\ M^{-1}$ (for an overall $\Delta G^{\circ\prime} = -10.1$ kcal/mol). Binding is positively cooperative, as observed for α CD-EF, but lower in affinity. The apparent standard free energy of Ca^{2+} binding is 1.4 kcal/mol less favorable for β CD-EF at the 240 μM concentration employed for the analysis.

Qualitatively, then, the Ca^{2+}-binding properties of the isolated CD-EF fragments mirror those of the parent parvalbumins. Importantly, however, the magnitude of the difference in Ca^{2+} affinity is 2.1 kcal/mol smaller for the fragments than for the full-length proteins. The latter exhibit a $\Delta\Delta G^{\circ\prime}$ for Ca^{2+} binding of 3.8 kcal/mol in Hepes-buffered saline, at pH 7.4 (M. T. Henzl, J. D. Larson, and S. Agah, unpublished data). This finding supports our contention that the AB domain—and more specifically, the interaction between the AB domain and the CD-EF domain—contributes to the free-energy disparity.

Equilibrium dialysis experiments, at a single peptide concentration, paint a deceptively simple picture of Ca^{2+} binding. As the ITC analyses reveal, the system is substantially more complex because of linkage between Ca^{2+} binding and self-association. Preparatory to modeling the β CD-EF Ca^{2+} binding events, five titrations were performed—at several peptide concentrations and in the absence or presence of NTA.

Our initial model assumed binding of Ca^{2+} to the EF site of the CD-EF monomer; association of two singly bound monomers; and (highly) cooperative occupation of the remaining two sites (the CD sites) in the dimer. The assumption of preferential binding at the EF site was based on the much greater affinity displayed by the EF site in the intact rat β-PV. Adequate at low-to-moderate peptide concentrations, this model failed to accommodate data collected with 116 and 250 μM β CD-EF—presumably because of dimerization of the apo-peptide prior to Ca^{2+} binding. After amending the model to include this possibility, the satisfactory fit displayed in Figure 7 was obtained. Two other modifications were also examined, as described in Results, but neither yielded a significantly improved fit.

In support of the model, we note that the estimate of the apo-peptide dimerization constant ($K_D = 2670\ M^{-1}$) agrees well with the estimate obtained by sedimentation equilibrium ($2440\ M^{-1}$). The value of K_1 ($3.6 \times 10^3\ M^{-1}$) is also in reasonable agreement with the estimate of the first macroscopic Ca^{2+}-binding constant obtained by equilibrium dialysis (4.2×10^3).

As noted above, the first Ca^{2+}-binding event in α CD-EF is strongly exothermic. By contrast, the binding of Ca^{2+} to the apo β monomer is apparently endothermic ($\Delta H_1 = +2.12$ kcal/mol)—which suggests that this event does not provoke a molecule-wide reorganization in β CD-EF. This difference may be a reflection of net charge—estimated at −7 in α, −10 in β. Conceivably, binding of a single Ca^{2+} does not reduce repulsion in the β peptide sufficiently to permit acquisition of native structure.

Instead, the initial Ca^{2+} binding event (assumed to occur at the EF site) is believed to provoke a structural rearrangement that is limited to the vicinity of the binding site.

However, this local conformational change must then facilitate the interaction between monomers because it raises the association constant more than 5-fold—from 2670 to 13 600 M^{-1}. The subsequent Ca^{2+}-promoted dimerization event is strongly exothermic ($\Delta H_{1D} = -15.7$ kcal/mol), implying that the bulk of β peptide folding accompanies this step.

At sufficiently high concentration, the apo-monomers can dimerize. However, the putative enthalpy change for this event is substantially endothermic ($\Delta H_D = +5.6$ kcal/mol), suggesting that this self-association phenomenon does not provoke significant folding. It may instead merely reflect the dehydration of the associating surfaces.

Tb^{3+}-Binding Studies. In full-length rat β, the Tb^{3+} bound at the CD site has the greater fluorescence signal (*28*) because of more efficient energy transfer from Tyr-57 and Tyr-65. Because the majority of the fluorescence increase occurs during the second half of the titration, it is apparent that the two binding sites are occupied sequentially, with the EF site filling first. On the basis of the relative magnitudes of A_1 and A_2 in our titrations of β CD-EF, we conclude that this order of occupancy is maintained in the isolated CD-EF fragment.

It was possible to fit the Tb^{3+}-binding data to a two-site Adair equation (eq 5) and extract apparent Tb^{3+}-binding constants consistent with data collected at 5, 10, and 20 μM peptide concentrations: $K_1 = 1.1 \times 10^6$ M^{-1}; $K_2 = 1.3 \times 10^6$ M^{-1}. Recall that the corresponding Ca^{2+}-binding constants, determined at higher peptide concentrations, were substantially lower, 4.2×10^3 and 6.1×10^3 M^{-1}.

When 20 μM β CD-EF is titrated with Tb^{3+} in the presence of 5.0 mM Ca^{2+}, the curve is shifted to higher concentration because of competition by the divalent ion. The order of occupation, however, is apparently retained—i.e., the binding site associated with the smaller amplitude fluorescence signal (i.e., the EF site) fills first. Under these conditions, least-squares analysis yields $K_1 = 5.6 \times 10^5$ M^{-1} and $K_2 = 1.0 \times 10^5$ M^{-1}. Thus, in the presence of 5.0 mM Ca^{2+}, the first binding constant is reduced by 50% and the second by a factor of 13. Apparently, Ca^{2+} competes more effectively with the lanthanide ion at the CD site, a phenomenon noted previously during Eu^{3+}-binding studies on the full-length protein (*38*).

The Tb^{3+} complex of β CD-EF—in which both CD and EF sites are occupied—behaves as a dimer at loading concentrations as low as 30 μM, in the presence of 0.5 mM Tb^{3+}.

Comparison with Published Results. Our binding constants for rat α CD-EF are substantially lower than those determined by Permyakov et al. (*20*) for the CD-EF fragment from pike parvalbumin III, also an α isoform (Table 3). This finding suggests that the pike α CD-EF domain possesses innately higher Ca^{2+} affinity than either fragment from rat.

Thépault et al. (*21*) recently performed a detailed structural analysis of rat α CD-EF, by both X-ray crystallography and NMR. They found that the Ca^{2+}-bound fragment adopts a compact structure, despite the loss of several contacts that exist in the full-length protein. Most of the parvalbumin fold is retained, with the exception of a large conformational change involving the DE linker region. Whereas this region occupies an external position in the full-length protein, in the fragment it has rotated approximately 19° closer to the hydrophobic core. This movement decreases the accessibility of the hydrophobic surface, which would otherwise be exposed by deletion of the AB domain.

Table 3: Binding Affinities for Pike and Rat Parvalbumins and Their CD-EF Fragments

protein	sample	reference	K_1 (M^{-1})	K_2 (M^{-1})	$\Delta G^{\circ\prime}_{total}$ (kcal/mol)
pike α	CD-EF	*20*	1.2×10^6	1.0×10^7	−17.8
	full-length protein	*20*	4.0×10^8	6.3×10^8	−23.6
rat α	CD-EF	*21*	1.0×10^6	2.5×10^5	−15.5
	CD-EF	this paper	3.7×10^3	8.6×10^4	−11.6
	full-length protein	this paper	2.5×10^8	6.1×10^7	−22.0
rat β	CD-EF	this paper	4.2×10^3	6.1×10^3	−10.1
	full-length protein	this paper	2.2×10^7	1.2×10^6	−18.2

The disparate self-association tendencies of the α and β fragments could conceivably reflect differences in the positioning of the linker region. It may be that, in β CD-EF, the linker adopts a conformation more closely resembling that of the full-length protein, thereby leaving the hydrophobic surface more accessible. The possibility that the spatial orientation of the linker is sensitive to the identities of residues 59 and 60 deserves exploration. Whereas both are glutamate in rat α, aspartate and glycine occupy these positions in rat β.

Thépault et al. did not comment on the tendency for α CD-EF to self-associate. On the basis of our results, we would predict significant dimerization of the Ca^{2+}-bound protein at NMR concentrations (ca. 1 mM). Perhaps the self-association phenomenon is suppressed under their NMR conditions—10% D_2O, pH 6.5, with no added salts or buffer. Similarly, no overt evidence of dimerization was reported for the crystal structure, although the authors noted that the crystals were very densely packed, with 52% of the solvent-accessible surface covered by crystal contacts.

Finally, Thépault et al. also reported Ca^{2+} binding constants for rat α CD-EF, included in Table 3. Their values, determined by fluorescence-based titration of Ca^{2+}-bound peptide with EGTA, are significantly higher than those we observe. However, because the data were omitted, and because minimal experimental detail was provided, it is difficult to gauge the uncertainty in their analysis.

CONCLUSIONS

Data for pike α and rat α and β indicate that parvalbumin CD-EF domains can exhibit diverse divalent ion-binding properties. The Ca^{2+} affinity reported for the pike CD-EF fragment is substantially higher than that of either rat isoform, and the overall Ca^{2+}-binding constant for rat α CD-EF is more than an order of magnitude larger than that of the rat β fragment. Potential explanations for the reduced Ca^{2+} affinity of the isolated β CD-EF fragment include its higher electrostatic free energy and/or the presence of aspartate, rather than glutamate, at the $-x$ ligation position in the CD binding loop. The relative Ca^{2+} affinities of the α and β CD-EF fragments qualitatively mirror those of the full-length proteins. However, the disparity in standard binding free energy is much smaller (1.4 vs 3.8 kcal/mol), consistent with a role for the AB domain in modulating divalent ion affinity.

Despite its higher net charge, rat β CD-EF dimerizes more readily than α CD-EF. Because this tendency is greatly

enhanced by Ca^{2+} (or Tb^{3+}), β CD-EF metal ion affinity is dependent on peptide concentration. The disparate self-association tendencies of the α and β fragments may reflect a conformational difference involving the linker region (residues 61−80 in the full-length protein).

As reported previously for α CD-EF (*21*), the β fragment is disordered in the Ca^{2+}-free form. At any given Ca^{2+} concentration, the α isoform is more stable, consistent with its greater Ca^{2+} affinity. However, the β CD-EF stability displays a greater concentration-dependence, consistent with its greater proclivity for dimerization.

The dependence of β CD-EF stability and Ca^{2+} affinity on peptide concentration illustrates the importance of assessing the self-association behavior of a system. Quantitative analysis of the β AB/CD-EF interaction will need to include the propensity of the isolated CD-EF fragment to dimerize.

APPENDIX

Derivation of the Model Used for Analysis of the β CD-EF ITC Data. The ligation state for a self-associating macromolecule is specified by the number of associated monomers, *i*, and the number of bound ligands, *j*. In general, the heat of formation of a particular macrostate equals

$$Q_{i,j} = \Delta H_{i,j}\alpha_{i,j} \tag{12}$$

where $\Delta H_{i,j}$ is the molar enthalpy change for formation of that state, and $\alpha_{i,j}$ is the species fraction for that state. The species fractions are given by expressions of the form

$$\alpha_{i,j} = (i\beta_{i,j}M^i x^j)/PF \tag{13}$$

where $\beta_{i,j}$ is the overall equilibrium constant for formation of the *i*,*j* state, *M* is the monomer concentration, *x* is the ligand concentration, and *PF* is the partition function for the system. In general, the cumulative heat of binding after the *n*th addition of titrant is given by the general expression

$$Q_n = \sum_{i=1,kj=1,p}\sum Q_{i,j} = \sum_{i=1,kj=1,p}\sum \Delta H_{i,j}\alpha_{i,j} \tag{14}$$

where the summations are taken over the *k* association states and *p* ligation states.

In the present case, we assume that only the following states are significantly populated: *M*, M_2, *M*Ca, $(M\text{Ca})_2$, and $(M\text{Ca}_2)_2$. The partition function for this system is then given by the following expresssion:

$$PF = M + 2K_D M^2 + K_1 Mx + 2K_{1D}(K_1 Mx)^2 + 2K_{D2}K_D M^2 x^2 + 2K_{D4}K_{1D}(K_1 M)^2 x^4 \tag{15}$$

where *M* is the concentration of the β CD-EF monomer (the reference species), *x* is the Ca^{2+} concentration, K_D is the dimerization constant for the apo-monomer, K_1 is the monomer Ca^{2+}-binding constant, K_{1D} is the dimerization constant for the singly bound monomer, K_{D2} is the constant governing the cooperative binding of two Ca^{2+} to the apo-dimer, and K_{D4} is the constant governing the cooperative binding of the final two Ca^{2+} ions. The individual terms in the equation reflect the contribution of each of the five states to the overall partition function.

The final expression for the cumulative heat of binding, following the *n*th addition, then becomes

$$Q_n = M_t V_o(2H_D K_D M^2 + H_1 K_1 Mx + (2H_1 + H_{1D})(2K_{1D}(K_1 Mx)^2) + (H_D + H_{D2})(2K_{D2}K_D M^2 x^2) + (2H_1 + H_{1D} + H_{D4})(2K_{2D}K_{1D}(K_1 M)^2 x^4))/PF \tag{16}$$

In the presence of NTA, the model includes an additional term to account for Ca^{2+} binding to the competitive ligand (cf., the first term in eq 10). Having developed an expression for the cumulative heat of binding, the heat associated with the *n*th injection is then calculated with eq 2.

NOTE ADDED AFTER ASAP

In the version published on the Web 03/01/2003, eq 1 and Figure 8 were incorrect. The final version was published 03/25/03.

REFERENCES

1. Kretsinger, R. H. (1980) Structure and Evolution of Calcium Modulated Proteins, *CRC Crit. Rev. Biochem. 8*, 115−164.
2. Celio, M. R., Pauls, T., and Schwaller, B. (1996) *Guidebook to the Calcium-Binding Proteins*, Oxford University Press, New York.
3. Seamon, K. B., and Kretsinger, R. H. (1983) Calcium-Modulated Proteins, in *Calcium in Biology* (Spiro, T. G., Ed.) pp 3−51, John Wiley and Sons, New York.
4. Wnuk, W., Cox, J. A., and Stein, E. A. (1982) Parvalbumins and other soluble high-affinity calcium-binding proteins from muscle, *Calcium Cell. Func. 2*, 243−278.
5. Kretsinger, R. H., and Nockolds, C. E. (1973) Carp Muscle Calcium-binding Protein. II. Structure Determination and General Description, *J. Biol. Chem. 248*, 3313−3326.
6. Goodman, M., and Pechère, J.-F. (1977) The evolution of muscular parvalbumins investigated by the maximum parsimony method, *J. Mol. Evol. 9*, 131−158.
7. Nakayama, S., Moncrief, N. D., and Kretsinger, R. H. (1992) Evolution of EF-hand calcium-modulated proteins. II. Domains of several subfamilies have diverse evolutionary histories, *J. Mol. Evol. 34*, 416−448.
8. Fohr, U. G., Weber, B. R., Muntener, M., Staudenmann, W., Hughes, G. J., Frutiger, S., Banville, D., Schafer, B. W., and Heizmann, C. W. (1993) Human alpha and beta parvalbumins. Structure and tissue-specific expression, *Eur. J. Biochem. 215*, 719−727.
9. Muntener, M., Kaser, L., Weber, J., and Berchtold, M. W. (1995) Increase of skeletal muscle relaxation speed by direct injection of parvalbumin cDNA, *Proc. Natl. Acad. Sci. U.S.A. 92*, 6504−6508.
10. Schwaller, B., Dick, J., Dhoot, G., Carroll, S., Vrbora, G., Nicotera, P., Pette, D., Wyss, A., Bluethmann, H., Hunziker, W., and Celio, M. R. (1999) Prolonged contraction-relaxation cycle of fast-twitch muscles in parvalbumin knockout mice, *Am. J. Physiol. 276*, 395−403.
11. Caillard, O., Moreno, H., Schwaller, B., Llano, I., Celio, M. R., and Marty, A. (2000) Role of the calcium-binding protein parvalbumin in short-term synaptic plasticity, *Proc. Natl. Acad. Sci. U.S.A. 97*, 13372−13377.
12. Henzl, M. T., Shibasaki, O., Comegys, T. H., Thalmann, I., and Thalmann, R. (1997) Oncomodulin is Abundant in the Organ of Corti, *Hear. Res. 106*, 105−111.
13. Sakaguchi, N., Henzl, M. T., Thalmann, I., Thalmann, R., and Schulte, B. A. (1998) Oncomodulin is Expressed Exclusively by Outer Hair Cells in the Organ of Corti, *J. Histochem. Cytochem. 46*, 29−39.
14. Epstein, P., Means, A. R., and Berchtold, M. W. (1986) Isolation of a rat parvalbumin gene and full length cDNA, *J. Biol. Chem. 261*, 5886−5891.
15. Gillen, M. F., Banville, D., Rutledge, R. G., Narang, S., Seligy, V. L., Whitfield, J. F., and MacManus, J. P. (1987) A complete

complementary DNA for the oncodevelopmental calcium-binding protein, oncomodulin, *J. Biol. Chem. 262*, 5308−5312.
16. Pauls, T. L., Durussel, I., Cox, J. A., Clark, I. D., Szabo, A. G., Gagne, S. M., Sykes, B. D., and Berchtold, M. W. (1993) Metal Binding Properties of Recombinant Rat Parvalbumin Wild-type and F102W Mutant, *J. Biol. Chem. 268*, 20897−20903.
17. Eberhard, M., and Erne, P. (1994) Calcium and Magnesium Binding to Rat Parvalbumin, *Eur. J. Biochem. 222*, 21−26.
18. Hapak, R. C., Lammers, P. J., Palmisano, W. A., Birnbaum, E. R., and Henzl, M. T. (1989) Site-specific Substitution of Glutamate for Aspartate at Position 59 of Rat Oncomodulin, *J. Biol. Chem. 264*, 18751−18760.
19. Cox, J. A., Milos, M., and MacManus, J. P. (1990) Calcium- and Magnesium-binding Properties of Oncomodulin, *J. Biol. Chem. 265*, 6633−6637.
20. Permyakov, E. A., Medvedkin, V. N., Mitin, Y. V., and Kretsinger, R. H. (1991) Noncovalent complex between domain AB and domains CD*EF of parvalbumin, *Biochim. Biophys. Acta 1076*, 67−70.
21. Thépault, M., Strub, M.-P., Cavé, A., Banères, J.-L., Berchtold, M. W., Dumas, C., and Padilla, A. (2001) Structure of rat parvalbumin with deleted AB domain: implications for the evolution of EF hand calcium-binding proteins and possible physiological relevance, *Proteins 45*, 117−128.
22. Pepper, D. S. (1998) Some Alternative Coupling Chemistries for Affinity Chromatography, in *Protein Protocols on CD-ROM* (Walker, J., Ed.) section 5.26, Humana Press, Totowa, NJ.
23. Stafford, W. F. (1992) Boundary analysis in sedimentation transport experiments: a procedure for obtaining sedimentation coefficient distributions using the time-derivative of the concentration profile, *Anal. Biochem. 203*, 295−301.
24. Bevington, P. R. (1969) *Data Reduction and Error Analysis for the Physical Sciences*, McGraw-Hill, New York.
25. Bevington, P. R., and Robinson, D. K. (1992) *Data Reduction and Error Analysis for the Physical Sciences*, 2nd ed., McGraw-Hill, New York.
26. Lakowicz, J. R. (1999) *Principles of Fluorescence Spectroscopy*, 2nd edition, Kluwer Academic/Plenum, New York.
27. Pace, C. N., Hebert, E. J., Shaw, K. L., Schell, D., Both, V., Krajcikova, D., Sevcik, J., Wilson, K. S., Dauter, Z., Hartley, R. W., and Grimsley, G. R. (1998) Conformational stability and thermodynamics of folding of ribonucleases Sa, Sa2, and Sa3, *J. Mol. Biol. 279*, 271−286.
28. Hogue, C. W. V., MacManus, J. P., Banville, D., and Szabo, A. G. (1992) Comparison of Terbium(III) Luminescence Enhancement in Mutants of EF Hand Calcium Binding Proteins, *J. Biol. Chem. 267*, 13340−13347.
29. MacManus, J. P., Hutnik, C. M. L., Sykes, B. D., Szabo, A. G., Williams, T. C., and Banville, D. (1989) Characterization and site-specific mutagenesis of the calcium-binding protein oncomodulin produced by recombinant bacteria, *J. Biol. Chem. 264*, 3470−3477.
30. Golden, L. F., Corson, D. C., Sykes, B. D., Banville, D., and MacManus, J. P. (1989) Site-specific mutants of oncomodulin. ^{1}H NMR and optical stopped-flow studies of the effect on the metal binding properties of an Asp59 → Glu59 substitution in the calcium-specific site, *J. Biol. Chem. 264*, 20314−20319.
31. Palmisano, W. A., Treviño, C. L., and Henzl, M. T. (1990) Site-specific replacement of amino acid residues within the CD binding loop of rat oncomodulin, *J. Biol. Chem. 265*, 14450−14456.
32. Henzl, M. T., Hapak, R. C., and Likos, J. J. (1998) Interconversion of the ligand arrays in the CD and EF sites of oncomodulin. Influence on Ca^{2+}-binding affinity, *Biochemistry 37*, 9101−9111.
33. Henzl, M. T., Wycoff, W. G., Larson, J. D., and Likos, J. J. (2002) ^{15}N nuclear magnetic resonance relaxation studies on rat β-parvalbumin and the penta-carboxylate variants, S55D and G98D, *Protein Sci. 11*, 158−173.
34. Skelton, N. J., Kordel, J., and Chazin, W. J. (1995) Determination of the solution structure of apo calbindin D9k by NMR spectroscopy, *J. Mol. Biol. 249*, 441−462.
35. VanScyoc, W. S., and Shea, M. A. (2001) Phenylalanine fluorescence studies of calcium binding to N-domain fragments of *Paramecium* calmodulin mutants show increased calcium affinity correlates with increased disorder, *Protein Sci. 10*, 1758−1768.
36. Finn, B. E., Evenas, J., Drakenberg, T., Waltho, J. P., Thulin, E., and Forsen, S. (1995) Calcium-induced structural changes and domain autonomy in calmodulin, *Nat. Struct. Biol. 2*, 777−783.
37. Li, M. X., Chandra, M., Pearlstone, J. R., Racher, K. I., Trigo-Gonzalez, G., Borgford, T., Kay, C. M., and Smillie, L. B. (1994) Properties of isolated recombinant N and C domains of chicken troponin C, *Biochemistry 33*, 917−925.
38. Henzl, M. T., and Birnbaum, E. R. (1988) Oncomodulin and parvalbumin. A comparison of their interactions with europium ion, *J. Biol. Chem. 263*, 10674−10680.

BI027060X